5th International Workshop on High-Order CFD Methods

January 6-7 2018 Kissimmee, USA

Abstract for the Onera NXO Finite Volume method

case I 1 : Inviscid Bow Shock upstream of a blunt body in supersonic flow

Jean-Marie Le Gouez[1]

Aerodynamics, Aeroacoustics, Aeroelasticity Department
ONERA - The French Aerospace Lab,
F- 92322 Châtillon France

1 NXO Code description

Discretization by cell-centered Finite Volume Method, 1 dof / eqn / cell, presented here in 2D.

Non compact method, based on the polynomial reconstruction over a wide stencil of either the fields of conservative variables W_i or the fields of components f_i of the flux tensor [1], projected in the direction of the interface $\vec{S} = [S_x, S_y]$, see fig 1.

$$\frac{\partial W_i}{\partial t} + \frac{\partial F_i}{\partial x} + \frac{\partial G_i}{\partial y} = 0$$

$$W = [\rho, \rho u, \rho v, \rho e_t]^T \qquad f_i = \frac{F_i S_x + G_i S_y}{\sqrt{S_x^2 + S_y^2}}$$

The fluxes scheme used here is a centered scheme close to the JST scheme [2]. The Finite Volume formulation reads:

$$\frac{\partial(\Omega \overline{W_i})}{\partial t} + \sum_{n=1}^{ni} S_n \left(\hat{f}_{i,nat} - \hat{f}_{i,diss} \right)_n = 0, \text{ with } \overline{W_i} = \frac{1}{\Omega} \iiint_{\Omega} W_i dV \text{ and } \hat{f}_i = \frac{1}{S} \iint_S f_i dS$$

The coefficients of the reconstructed polynomials P of degree k are linear combinations of the discrete fields in the cells [1]. They are projected as averages without limiting onto the interface, the resulting integral projection is a linear combination of the discrete fields, known as their volume average in the cells of the stencil : $\hat{\phi} = \Pi_{NXO}(\overline{\phi}) = \sum_{stencil} \lambda_s \overline{\phi}_s$.

The fields of interest can be either the conservative variables or the flux densities in the direction normal to the interface:

$\phi = W_i$ or f_i .

For each cell interface, the interpolations coefficients from volume averages to surface average λ are computed in the H-O metrics pre-processor, where the polynomial order k is adapted to the geometry and number of cells of the stencil; these coefficients can be used for a variety of upwind, characteristic-based or centred schemes [4].

[1] jean-marie.le_gouez@onera.fr, AIAA member.

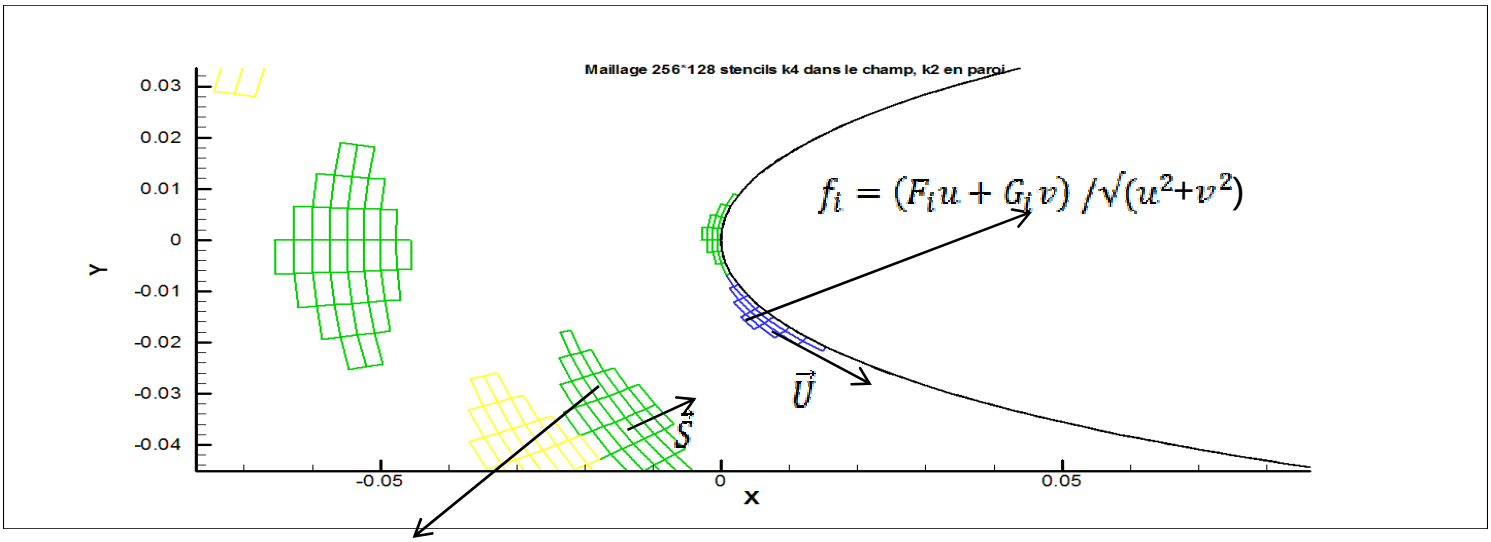

Fig 1 : Representation of typical boundary or field stencils for k2 to k5 reconstructions on full 2D bases of either conservative variables, eulerian fluxes or lagrangian fluxes

Here we write :

- $\hat{f}_{i,nat} = \dfrac{\hat{f}_{i,left} + \hat{f}_{i,right}}{2} = \dfrac{\sum_{s\in St,left} \lambda_{left,s}\, \bar{f}_{i,s} + \sum_{s\in St,right} \lambda_{right,s}\, \bar{f}_{i,s}}{2}$ is the mean of the reconstructed and face projected normal fluxes in the cells of the left and right stencil (2 stencils of arbitrary width centered respectively on the left and right cell on either side on the interface, highly overlapping). We define $\bar{f}_{i,s} = f_i\left(\overline{W}_{j,s}\right)$ which impacts the asymptotic order of the overall scheme [1].
- $\hat{f}_{i,diss} = \varepsilon_2\, \omega \hat{\delta} W_i^* - \varepsilon_4 \omega \hat{\delta}\hat{\delta}\hat{\delta} W_i^*$, where W_i^* uses the total enthalpy rather than the total energy in the energy equation, $W^* = [\rho, \rho u, \rho v, \rho h_t]^T$, then $\hat{\delta} W_i^*$ is an evaluation at high order of the first grid difference of W_i^* over the interface and $\hat{\delta}\hat{\delta}\hat{\delta} W_i^*$ that of the third difference. $\omega = \dfrac{|uS_x + vS_y|}{\sqrt{S_x^2 + S_y^2}} + a$ is the highest module of the eigenvalues of the flux Jacobian at the interface, computed for the stencil average Π_{NXO} of conservative variables, a the speed of sound.

The high order evaluations of the grid differences use a polynomial reconstruction over the union of the two cell-centered stencils, so it is possibly a degree higher than the cell-biased reconstructions used for the natural part $\hat{f}_{i,nat}$. Only the linear combination coefficients μ_1 and μ_3 analogous to λ are obtained from the interface projection of the first and third normal derivatives of the reconstructed polynomial, which are polynomials of degree k-1 and k-3.

If h is the grid size normal to the interface:

$$\hat{\delta} W_i^* = h \int_S \frac{\partial P_i^*}{\partial \upsilon} dS = h \sum_{St,left \cup St,right} \mu_{1s} \overline{W}_{i,s}^*$$

$$\hat{\delta}\hat{\delta}\hat{\delta} W_i^* = h^3 \int_S \frac{\partial^3 P_i^*}{\partial \upsilon^3} dS = h^3 \sum_{St,left \cup St,right} \mu_{3s} \overline{W}_{i,s}^*$$

Consistently with the Jameson scheme, the ε_2 coefficient contains a discontinuity detection formula and ε_4 is constant away from the discontinuity and related to ε_2 so that it vanishes near the discontinuity.

Boundary conditions

The boundary stencils are of reduced size (3 or 4 cells), and use a quadratic reconstruction for the extrapolation of conservative variables to the boundaries.

For all open boundaries a non-reflective BC is used, based on Riemann invariants. The reference field Mach number increases linearly over the first few thousand iterations then remains constant.

At the wall boundary, a compatibility relation is used. The HO extrapolated pressure P_{ext} is modified by a correction term proportional to the HO extrapolation of the normal velocity : $P_w = P_{ext} + \rho_{ext} a_{ext} U_{v,ext}$, with a the sound velocity.

Adaptation to the structured grids of the test case

The reconstruction and projection scheme is restricted on these grids to directional 1D stencils in the direction normal to the interface, so the only monomials of the base are powers of the normal coordinate (see figure 2 for a plot of some stencils).

The preprocessings are done successively with cell stencils of 5, 7 and 9 stencils enabling k-exact reconstructions from k2 to k5, since from our experience the WLSQ requests a ratio between the number of cells and the number of monomials higher than or equal to 1.5 . The exact cell node coordinates are used, so varying size of the cells in the stencil is accounted for.

The corresponding face stencils used for the artificial dissipation comprise 6, 8 or 10 cells, and enable to reconstruct k3 to k5 polynomials. The 6-cell face stencil is the smallest one that permits a k3 reconstruction and a high order expression of the third differences.

A typical set of coefficients associated to an interface is shown in table 1. The first two cells are the left and right ones, then they are at increasing distances from the interface.

The diagonal dominance is ensured by the high coefficient of the “upside” cell in the first two rows. The first and third difference coefficients are of the same order of magnitude and with correct signs. In table 2 the coefficients for an interface in the refined region shows that the coefficients are no longer symmetrical.

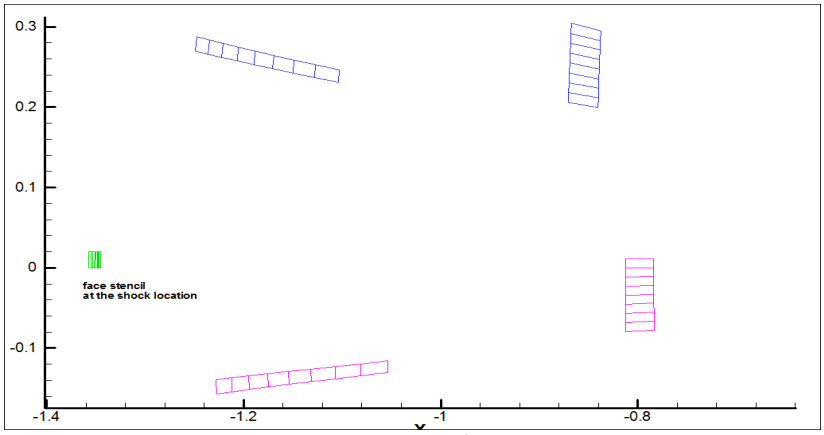

Fig. 2 Typical 8-cell face stencils

Cell number	λ_{left}	λ_{right}	$h\mu_1$	$h^3\mu_3$
6889	8.686790E-01	3.524098E-01	-9.145573E-01	1.189409E+00
6890	3.522242E-01	8.680207E-01	9.148241E-01	-1.190158E+00
6888	-2.313252E-01	-3.575830E-03	-6.769385E-02	-1.695131E-01
6891	-3.559571E-03	-2.306794E-01	6.728783E-02	1.711246E-01
6887	1.313760E-02	-7.945943E-03	1.676038E-02	-1.059340E-01
6892	-7.913174E-03	1.306851E-02	-1.666678E-02	1.053282E-01
6886	8.757148E-03	0.000000E+00	4.823821E-03	-2.164341E-02
6893	0.000000E+00	8.702156E-03	-4.778195E-03	2.138642E-02
Sum	1.000000E+00	1.000000E+00	7.742652E-14	3.258746E-13

Table 1. Typical table of coefficients for the 8-cell scheme

Cell number	λ_{left}	λ_{right}	$h\mu_1$	$h^3\mu_3$
18797	7.928224E-01	2.746035E-01	-7.901984E-01	8.435314E-01
19093	3.631856E-01	9.336806E-01	7.625114E-01	-4.200037E-01
18501	-1.462949E-01	1.748151E-02	-7.364388E-02	-2.629008E-01
19389	5.650325E-03	-2.379641E-01	1.233299E-01	-1.793107E-01
18205	-5.628299E-03	3.194552E-04	-7.385052E-04	-7.281388E-02
19685	-1.200030E-02	7.556028E-04	-1.387728E-02	7.143579E-02
17909	2.265183E-03	0.000000E+00	1.006295E-03	-1.422409E-02
19981	0.000000E+00	1.112340E-02	-8.389457E-03	3.428604E-02
Sum	1.000000E+00	1.000000E+00	8.658745E-14	4.251879E-13

Table 2 Table of coefficients for an interface in the region of grid refinement (normal shock)

Expression of the ε_2 and ε_4 coefficients

The discontinuity detector is based on an estimate of the total variation of pressure over the n_s cells of the face stencil (n_s = 6, 8 or 10), scaled by the minimal value of the pressure in the left and right cells adjacent to the interface:

$$\chi = \max\left(\frac{\sum_{s=1}^{n_s} |P_s - P_{av}|}{n_s \min(P_1, P_2)}, 10^{-3} \right)$$, where $P_{av} = \frac{1}{n_s}\sum_{s=1}^{n_s} P_s$. χ is found to vary in the range 10^{-3} to 10.

We need to adapt the coefficients, based on our experience of the behavior of the solver in this Mach 4 detached shock case. We introduce a single multiplicative coefficient c_{art} , varied between 0.065 to 0.100 to obtain a uniform convergence on all 5 grids and 3 stencil dimensions. It is found that ε_2 cannot vanish completely away from the discontinuity and needs to spread away from it. A background level is set and the spatial variation of χ is smoothed by using the log function, so

$\tau = 0.1 + \left(\frac{3 + \log_{10} \chi}{3} \right)^{1.75}$ varies typically from 0.1 to 2.0,

then $\varepsilon_2 = c_{art}\ \tau$ and $\varepsilon_4 = c_{art}\ max(0.3 - \tau, 0)$.

The spatial variation of ε_2 and ε_4 is illustrated on figure 3, for a run on grid2 with 8-cell stencils and k4 reconstruction.

Test case results

The exact analytical value of the pressure at the stagnation point is Pw,a = 15.0486314
The scheme is found more accurate on 8 cell stencils. We record the pressure at the stagnation point and its error, together with the rms error on total enthalpy, respectively on all grid cells and wall faces. The integral of the pressure force on the wall is also presented in table 3, and the CPU cost of the run in TauBench Units.

	Pw	E(Pw)	E(Ht)/grid	E(Ht)/wall	Wall x-Force	Cells = dof/eqn	Cost (TBU)
grd0	**15.050863**	**$2.23\ 10^{-3}$**	**$8.64\ 10^{-4}$**	**$9.85\ 10^{-4}$**	**2.93435**	**2220 (74*30)**	**7.3**
grd1	**15.041765**	**$6.87\ 10^{-3}$**	**$3.06\ 10^{-4}$**	**$5.91\ 10^{-5}$**	**2.92049**	**7922 (148*54)**	**77.8**
grd2	**15.048396**	**$2.36\ 10^{-4}$**	**$2.31\ 10^{-4}$**	**$6.40\ 10^{-6}$**	**2.91948**	**29008 (296*98)**	**790**
grd3	**15.049017**	**$3.85\ 10^{-4}$**	**$1.81\ 10^{-4}$**	**$9.21\ 10^{-7}$**	**2.91776**	**109740 (590*186)**	**6471**
grd4	**15.048587**	**$4.47\ 10^{-5}$**	**$5.53\ 10^{-5}$**	**$1.17\ 10^{-7}$**	**2.91729**	**427160 (1180*362)**	**69970**

Table 3: Results on the 5 grids with 8-cell stencils: k3 reconstructions of natural fluxes (reported on figure 17)

Table 4 gathers the same results for the runs on the three fused stencils widths (6-cell, 8-cell and 10-cell).
The solution with 8 cells is more accurate, especially on the finer grids; there is no further gain in using 10-cell stencils.

	Pw	E(Pw)	E(Ht)/grid	E(Ht)/wall	Wall x-Force	Cells = dof/eqn
grd0						
6-c	**15.050507**	**$1.88\ 10^{-3}$**	**$1.38\ 10^{-3}$**	**$1.53\ 10^{-3}$**	**2.93326**	
8-c	**15.050863**	**$2.23\ 10^{-3}$**	**$8.64\ 10^{-4}$**	**$9.85\ 10^{-4}$**	**2.93435**	**2220 (74*30)**
10-c	**15.021457**	**$2.72\ 10^{-2}$**	**$4.21\ 10^{-4}$**	**$9.57\ 10^{-4}$**	**2.93388**	
grd1						
6-c	**15.028278**	**$2.04\ 10^{-2}$**	**$8.24\ 10^{-4}$**	**$3.06\ 10^{-4}$**	**2.92046**	
8-c	**15.041765**	**$6.87\ 10^{-3}$**	**$3.06\ 10^{-4}$**	**$5.91\ 10^{-5}$**	**2.92049**	**7922 (148*54)**
10-c	**15.036790**	**$1.18\ 10^{-2}$**	**$3.49\ 10^{-4}$**	**$6.79\ 10^{-5}$**	**2.92491**	
grd2						
6-c	**15.043914**	**$4.71\ 10^{-3}$**	**$2.74\ 10^{-4}$**	**$5.30\ 10^{-5}$**	**2.91894**	
8-c	**15.048396**	**$2.36\ 10^{-4}$**	**$2.31\ 10^{-4}$**	**$6.40\ 10^{-6}$**	**2.91948**	**29008 (296*98)**
10-c	**15.049917**	**$1.29\ 10^{-3}$**	**$2.53\ 10^{-4}$**	**$7.55\ 10^{-6}$**	**2.92071**	
grd3						
6-c	**15.049261**	**$6.30\ 10^{-4}$**	**$2.12\ 10^{-4}$**	**$1.18\ 10^{-5}$**	**2.91794**	
8-c	**15.049017**	**$3.85\ 10^{-4}$**	**$1.81\ 10^{-4}$**	**$9.21\ 10^{-7}$**	**2.91776**	**109740 (590*186)**
10-c	**15.049549**	**$9.18\ 10^{-4}$**	**$1.59\ 10^{-4}$**	**$1.47\ 10^{-6}$**	**2.91833**	
grd4						
6-c	**15.048737**	**$1.06\ 10^{-4}$**	**$9.16\ 10^{-5}$**	**$2.90\ 10^{-6}$**	**2.91751**	
8-c	**15.048587**	**$4.47\ 10^{-5}$**	**$5.53\ 10^{-5}$**	**$1.17\ 10^{-7}$**	**2.91729**	**427160 (1180*362)**
10-c	**15.048925**	**$2.93\ 10^{-4}$**	**$7.92\ 10^{-5}$**	**$2.44\ 10^{-6}$**	**2.91770**	

Table 4: Results on the 5 grids with 3 different stencil widths: k2 / k3 / k5 reconstructions of natural fluxes. see Figure 17

Comments on the 8-cell solution

1/ Error on total enthalpy (per unit mass) over the whole grid.
The rate of spatial convergence of this rms error is of the order of 1, its value is on average 12 times lower than the error of the reference 2nd order FV solver with a centred scheme and 120 lower than the HLLE results of this solver.
The fact that the artificial diffusion in the energy equation is based on first and third differences of the total enthalpy per unit volume rather than total energy is found beneficial. The usage of a high order difference formula in the artificial diffusion as for the natural Euler fluxes, with the μ coefficients involving 6 to 10 points in the first and third differences, rather than simpler 2 or 4 point formulas of lower order is found worthwhile, without any more theoretical argument to support this choice.

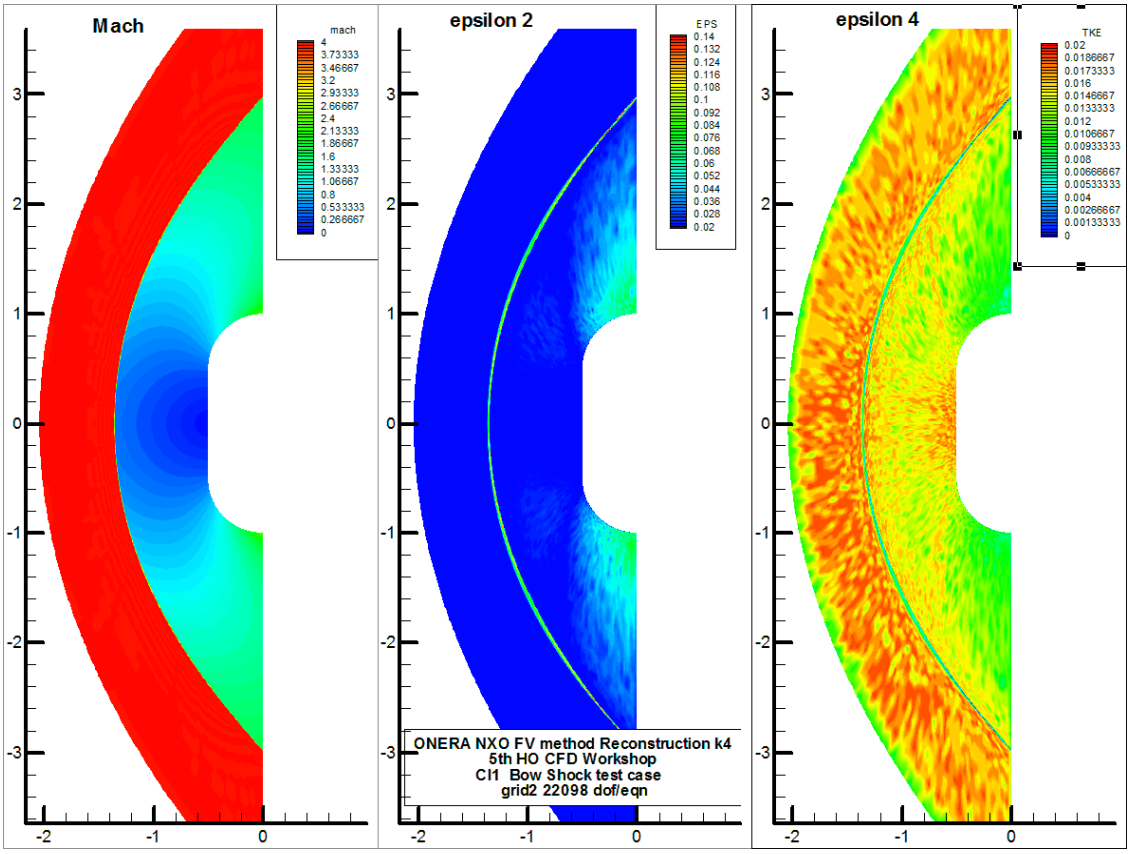

Fig.3 Fields of $\mathcal{E}_2$ and $\mathcal{E}_4$ in the 8-cell stencil case on grid2

The main point that allows a higher accuracy is the stencil-reconstruction of face normal fluxes rather than conservative variables. These fluxes are continuous over the stencil across normal shocks when the grid is fitted to them (see Fig 4), although their space derivatives in the flow direction are not (the longitudinal fluxes along x start to decrease linearly towards the wall after the shock). This stencil HO reconstruction of the fluxes transfers the error in the regions where the shock is not normal and less intense. The error trace in total enthalpy over the shock is reported on figure 14, its amplitude if of the order of 1% of the reference level and decreases a little on finer grids. The error is located in only 2 cells across the shock as shown on figure 18.

2/ Error on pressure at the stagnation point

The space convergence is plotted on figure 17. The rate of spatial convergence of this local error is of the order of 1.5, and its magnitude is about 10 times lower than the 2nd order FV solution on each grid. The solutions by the NXO method on grid1 and grid3 show higher errors than the global trend, this is probably due to the fact that these grids are not refined in exactly the same regions than the other ones and the shock location can be offset by 5 to 8 cells from the highest refinement zone. The extrapolation of field flow variables to the wall is of order 2, but only in the wall normal direction. Using 2D stencils near the wall, as shown on figure 1, and a curvilinear integration in the pre-processor might enhance the accuracy of the boundary treatment.

3/ Error on total enthalpy over the wall

The rate of spatial convergence of this rms error is of the order on 3.26 and rather uniform from grid0 to grid4.

4/ Rate of convergence of the control volume residuals

The solution is evolved with the 3-stage RK iteration scheme proposed by Shu and Osher [3], using a local pseudo-time, computed for a cfl of 0.75 to 1. The convergence of the residuals of all equations is uniform, after the initial phase of the computation where the Mach number is increased steadily in the far-field BC. This is presented on figure 5.

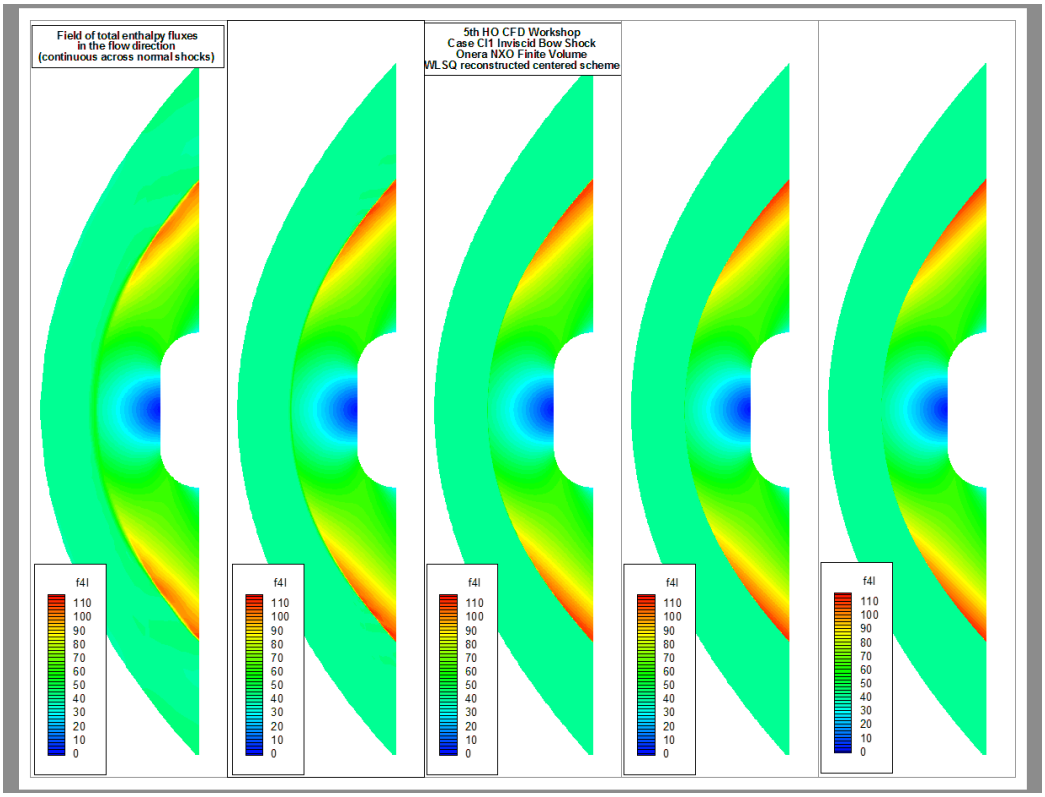

Fig. 4 Field of flux density tensor projected in the direction of the flow, for the energy equation, on 5 grids

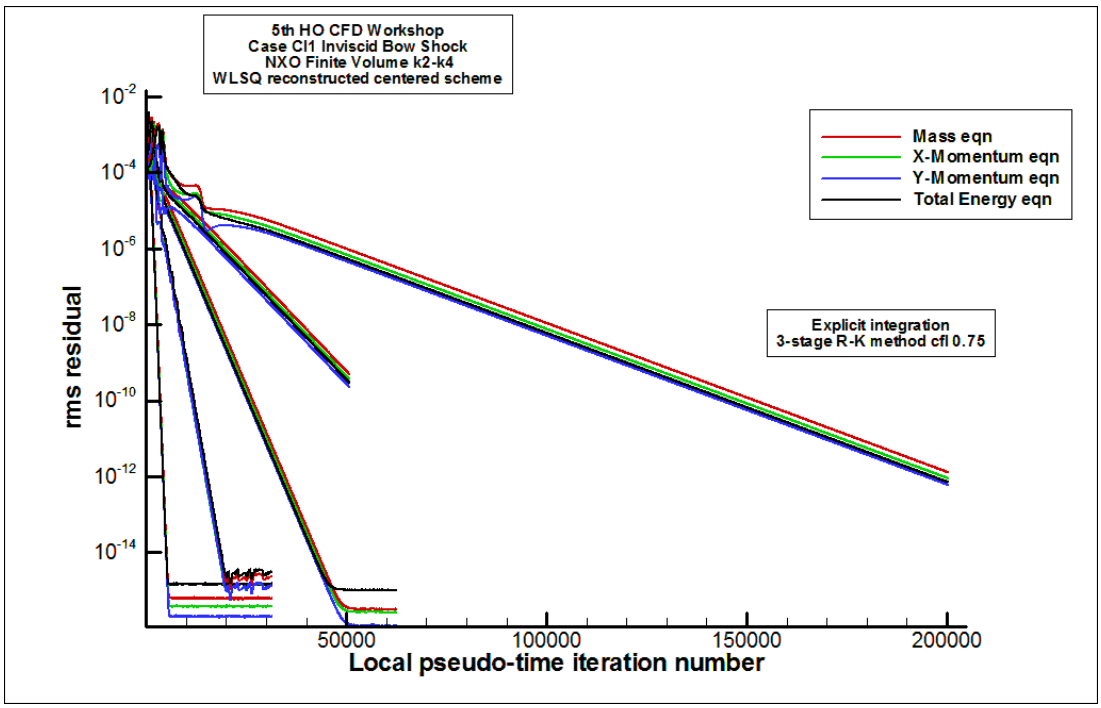

Fig.5 Convergence of the rms residuals of the 4 conservation equations for the 5 grids

5/ Convergence of the error indicators

Figures 6 to 8 show the convergence of the error indicators with the pseudo-time iteration number. On Figure 7, the error on the pressure at the stagnation point is higher on grid 1 than on grid0 and higher on grid3 than on grid2.

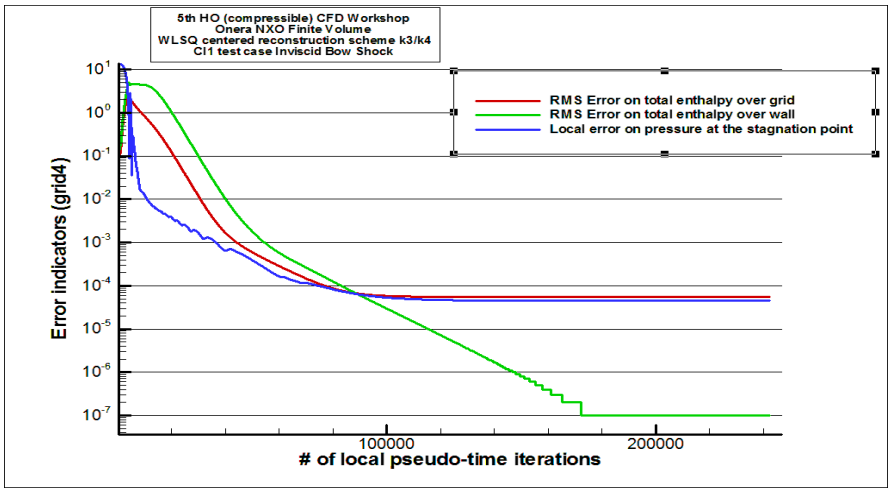

Fig.6 Convergence of the 3 error indicators for the fine grid run

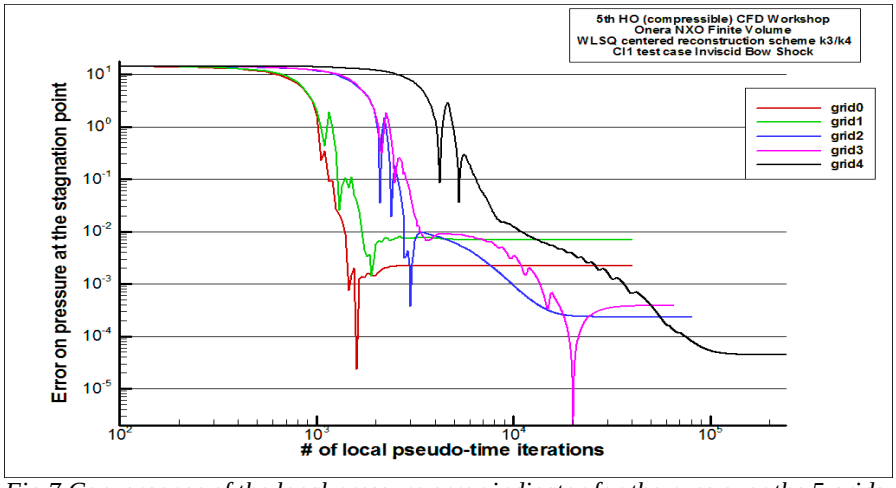

Fig.7 Convergence of the local pressure error indicator for the runs over the 5 grids. Spikes indicate a change of sign of the error

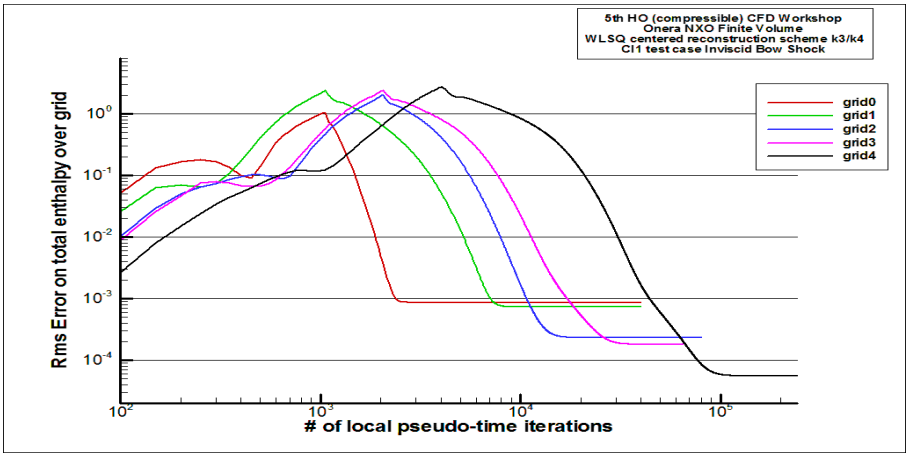

Fig.8 Convergence of the total enthalpy rms error over the grid, for all 5 runs

6/ Flow fields

Figures 9 to 12 plot the total enthalpy and its error field, then the pressure field and iso_Mach lines on all 5 grids.

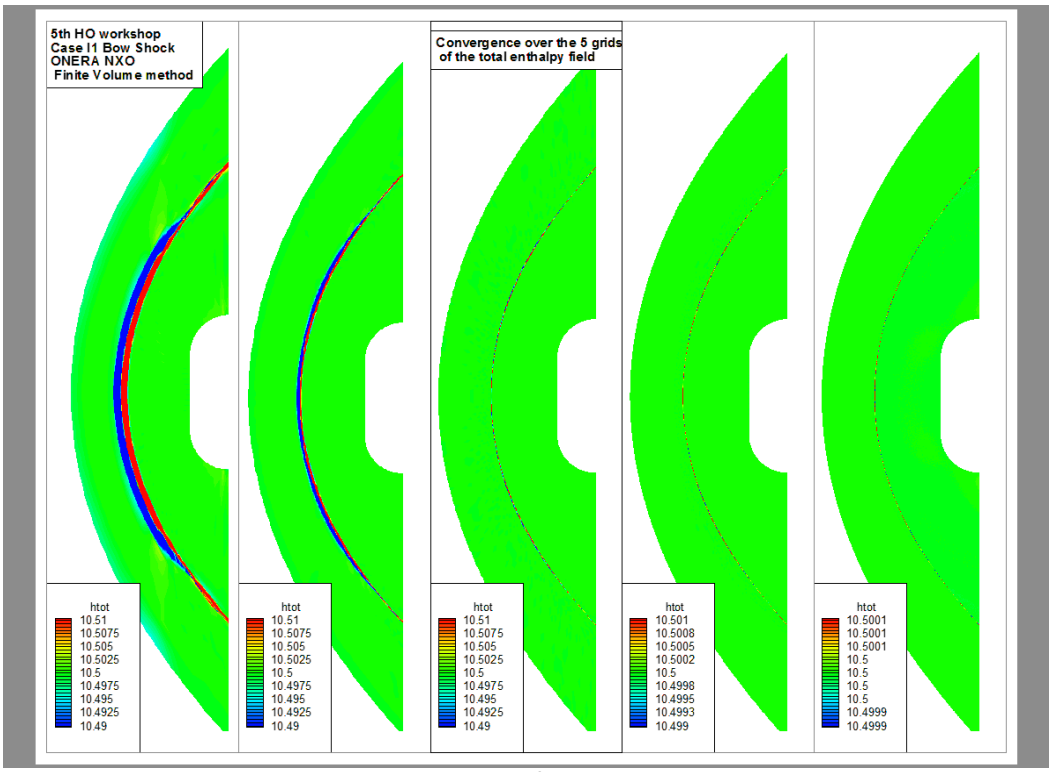

Fig.9 Total enthalpy fields over the 5 grids

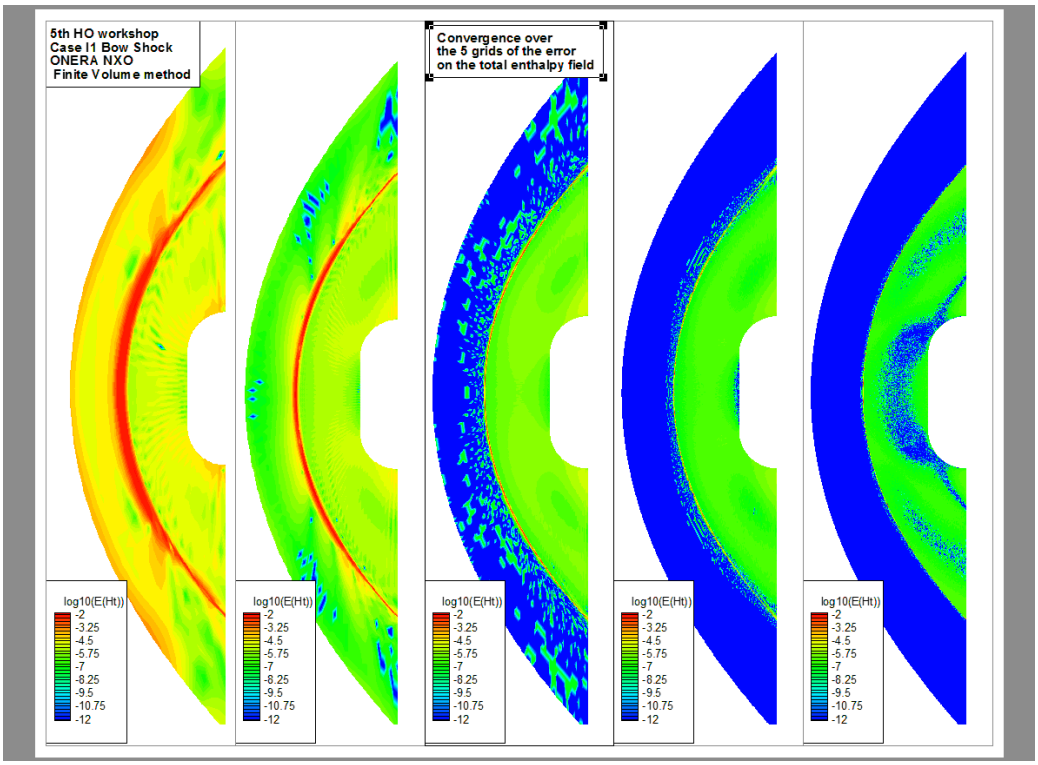

Fig.10 Log of the total enthalpy error fields over the 5 grids

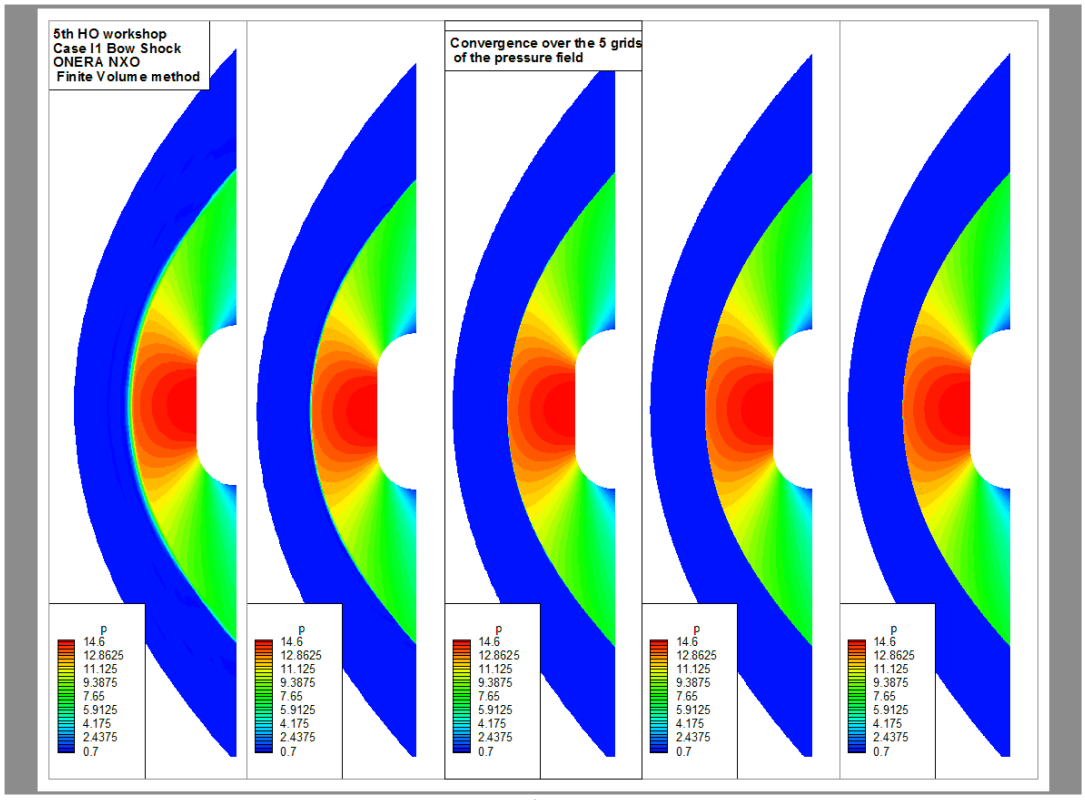

Fig.11 Pressure fields on the 5 grids

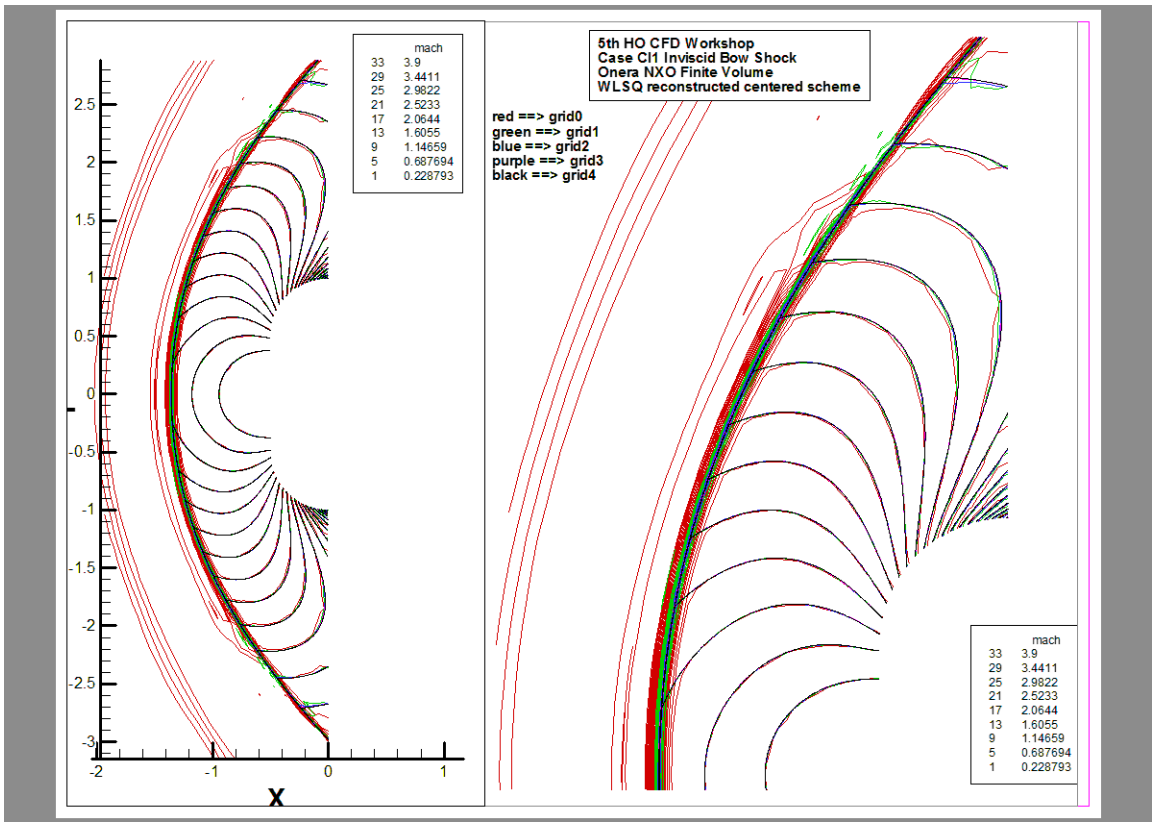

Fig.12 Iso-Mach lines on the 5 grids

7/ Flow fields variation along the symmetry axis

The shock location and the aerodynamics quantities at the stagnation point exhibit fast convergence with the grid refinement.

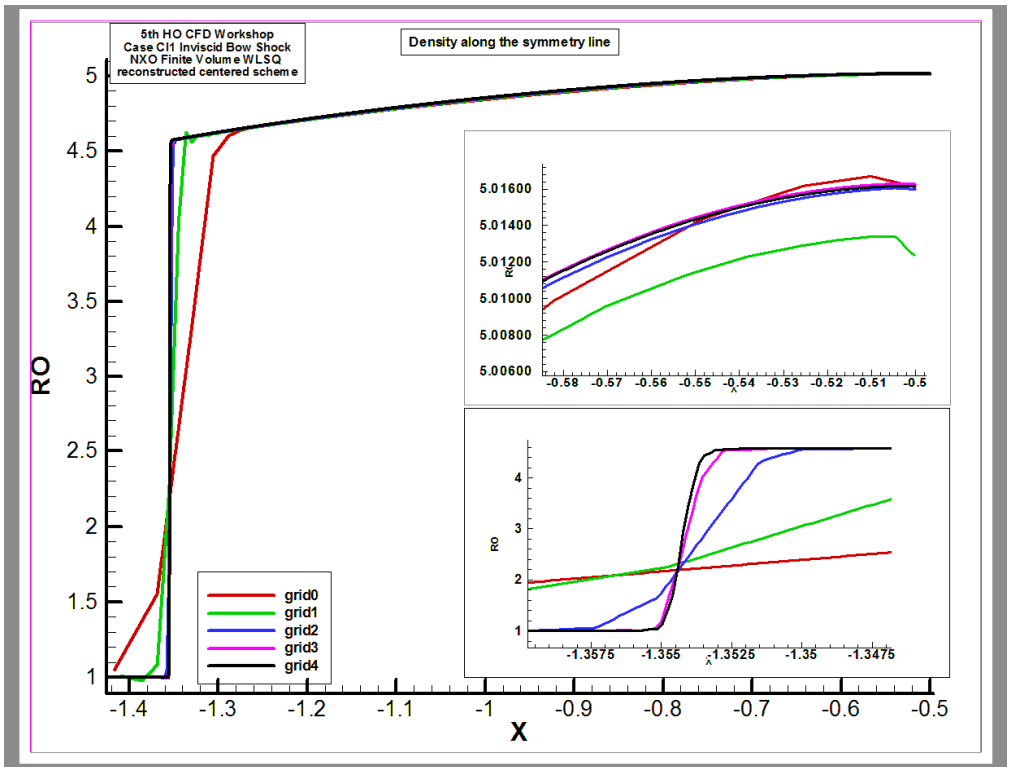

Fig.13 Density on the symmetry axis (zooms on the shock region and the stagnation point)

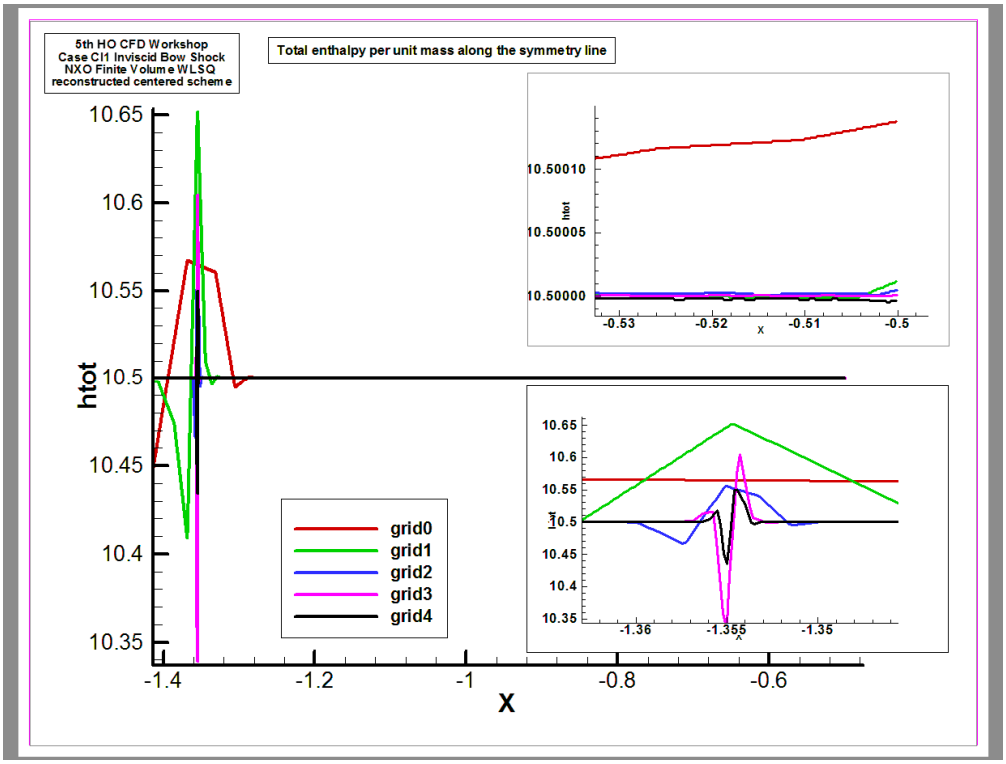

Fig.14 Total enthalpy on the symmetry axis (zooms on the shock region and the stagnation point)

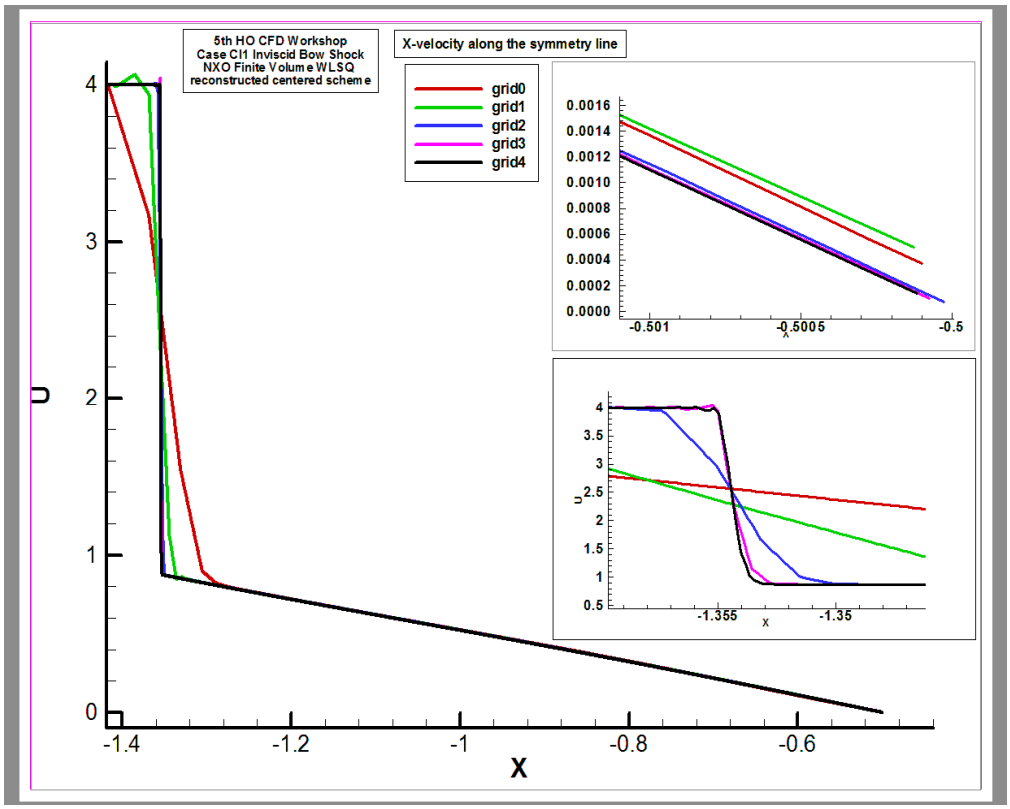

Fig.15 X-velocity on the symmetry axis (zooms on the shock region and the stagnation point)

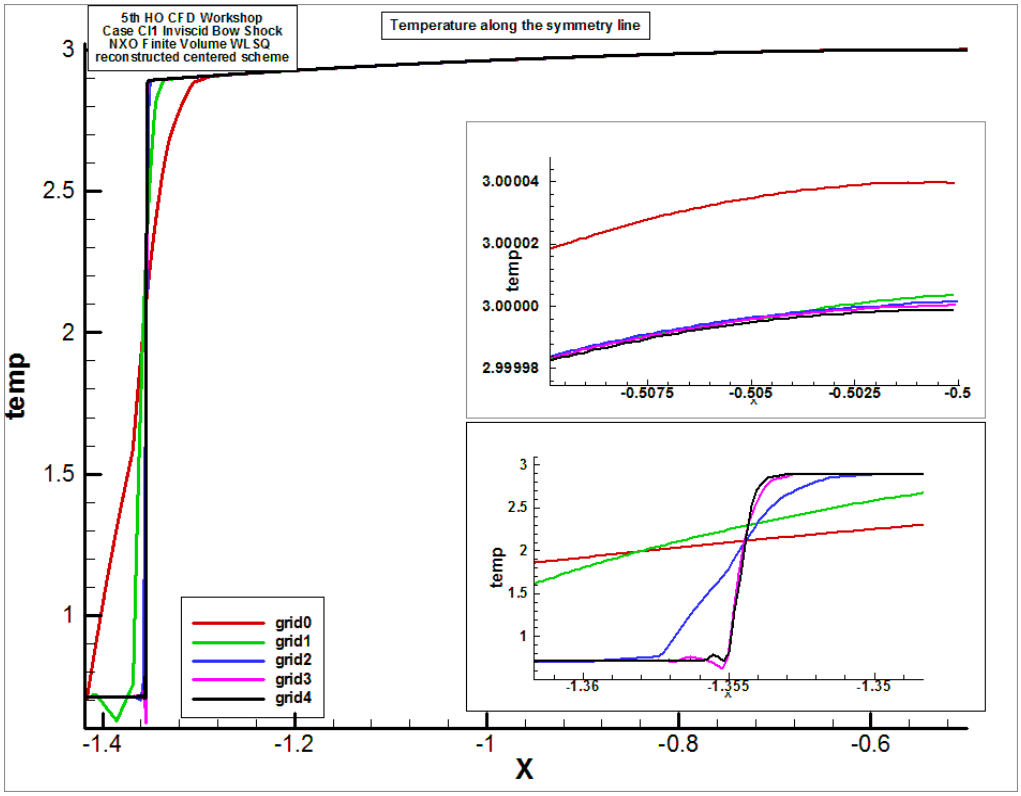

Fig.16 Temperature on the symmetry axis (zooms on the shock region and the stagnation point)

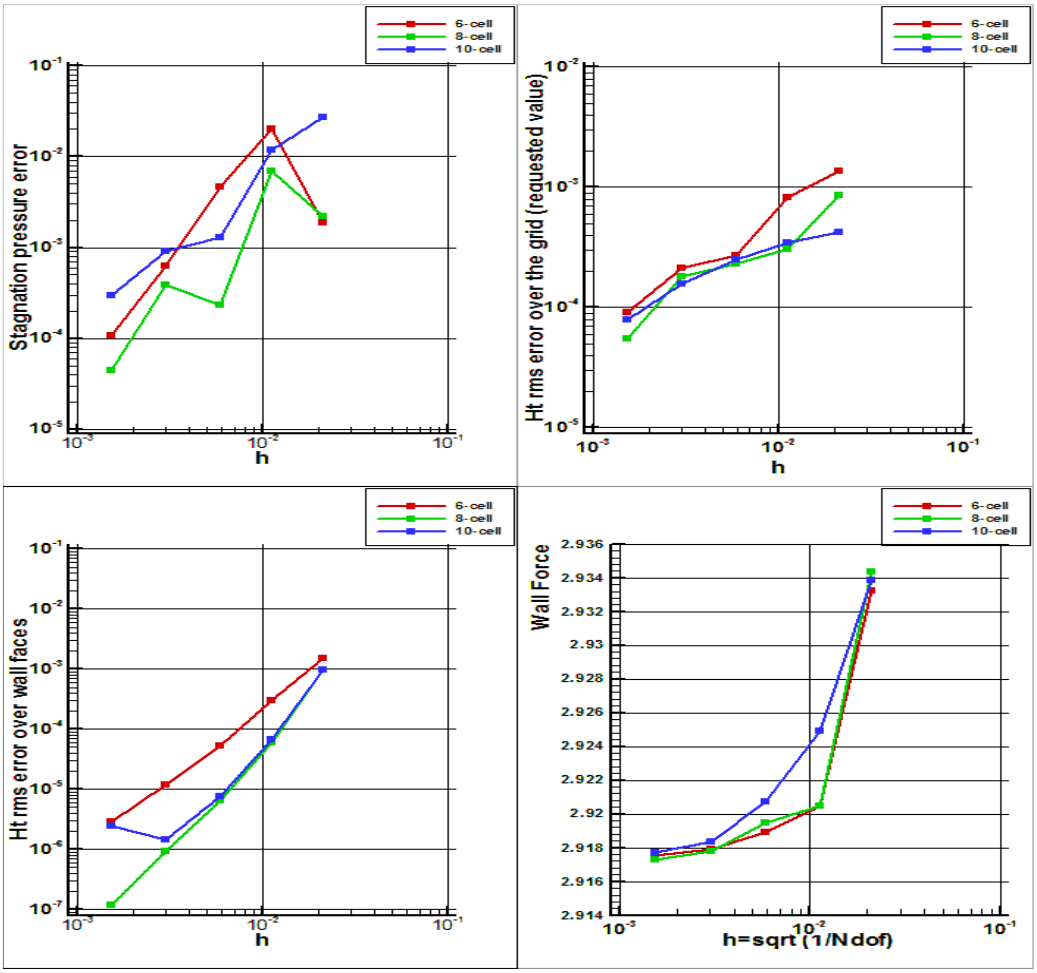

Fig.17 Error indicators and Wall x-force function of the mesh size

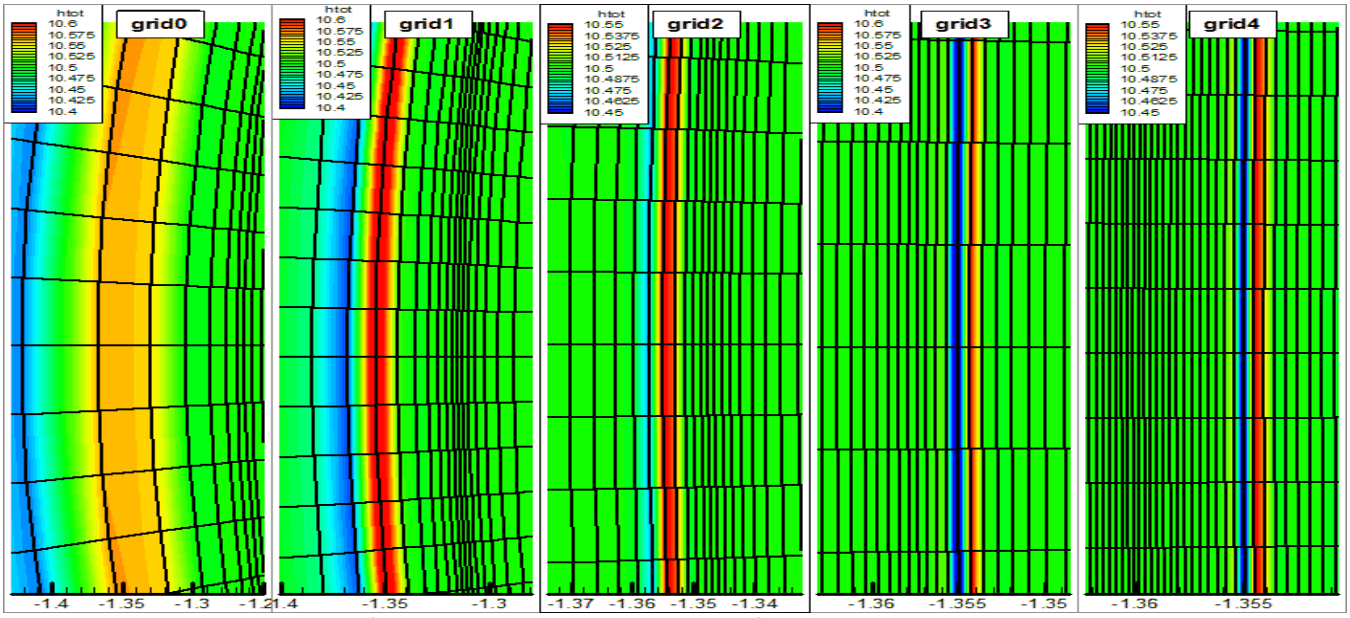

Figure 18 Location of the shock with respect to the grid refinement (total enthalpy over / undershoots)
The shock position converges to x=-1.355

REFERENCES

[1] J.M. Le Gouez, “High-Order Overset Interpolation via Weighted Least-Square Polynomial Reconstruction for Finite Volume CFD”, AIAA Paper 2016_2051, SciTech 2016, 4-8 Janvier 2016, San Diego, Californie.

[2] Antony Jameson. "Origins and Further Development of the Jameson–Schmidt–Turkel Scheme", AIAA Journal, Vol. 55, No. 5 (2017), pp. 1487-1510.

[3] C.-W. Shu, S. Osher, Efficient implementation of essentially non-oscillatory shock-capturing schemes, J. Comput. Phys. 77 (1988) 439-471.

[4] J.M. Le Gouez, Researchgate project 2016
https://www.researchgate.net/project/NextFlow-Spatially-HO-Finite-Volume-method-for-Compressible-Navier-Stokes